Hindawi
Mathematical Problems in Engineering
Volume 2018, Article ID 6141035, 12 pages
https://doi.org/10.1155/2018/6141035

Research Article

Influence of Shaft Torsional Stiffness on Dynamic Response of Four-Stage Main Transmission System

Yuan Chen,[1,2] Rupeng Zhu ,[1] Guanghu Jin,[1] and Yeping Xiong[2]

[1]*College of Mechanical and Electrical Engineering, Nanjing University of Aeronautics and Astronautics, Nanjing 210016, China*
[2]*Engineering and the Environment, University of Southampton, Boldrewood Innovation Campus, Southampton SO16 7QF, UK*

Correspondence should be addressed to Rupeng Zhu; rpzhu@nuaa.edu.cn

Received 5 October 2017; Revised 19 December 2017; Accepted 1 January 2018; Published 8 April 2018

Academic Editor: Jussi Sopanen

Dynamic response analysis has potential for increasing fatigue life of the components in the transmission of a multistage main transmission system. The calculated data can demonstrate the influence of shaft torsional stiffness on dynamic characteristics of the system. Detecting key shafts of the system and analyzing their sensitivity are important for the design of four-stage helicopter gear box. Lumped mass method is applied for dynamic modeling and Fourier method is used to solve differential equation of the system. Results of the analysis indicate that key shafts can be designed carefully to improve the performance of the transmission system.

1. Introduction

Helicopter transmission dynamic analysis is important to helicopter vibration system because helicopters has long transmission chain. Lumped mass method has been developed to establish the vibration based model. Various dynamic factors, such as time-varying meshing stiffness, clearance, and synthetic transmission error, are taken into account in each branch of the system. Fourier series method is applied to solve differential equation of motion, so dynamic response influenced by shaft torsional stiffness is calculated to analyze vibration characteristics. Sensitivity analysis method is developed and implemented in four-stage main transmission system to detect the key shaft.

The four-stage main transmission system has potential for carrying heavy load compared to other reducer system, and it is particularly relevant in complex dynamic behavior in three-engine helicopters. The system structure is extremely complicated: it has multiple branches of input and output, along with long transmission chain which includes numerous gears and accessories. Therefore, it is urgent and meaningful to analyze and study its vibration characteristics; predicting dynamic response and detecting key shaft might protect the whole system from further damage [1, 2]. The input speed and torque are greatly high in this system which could lead to transmission failure. Several studies have concluded that transmission malfunction caused helicopter accidents under severe working condition [3, 4]. In this case, key shafts should be predicted accurately and designed carefully.

For helicopter main transmission system, scholars established the complex multishaft system based on finite element method [5] and analyzed the influence of meshing stiffness, installation angle, spiral angle, and bearing stiffness on the natural characteristics [6] through numerous methods, such as impedance matching method [7] and whole transfer matrix method [8, 9]. The shaft sensitivity analysis dates back to the 1980s. These studies explored the sensitivity of torsional modes and maximum torsional torques to turbine-generator shaft mechanical parameters [10–12], which provided references for detecting key shafts in this paper.

The main part of four-stage transmission system is planetary gear chain of main transmission system. In the 1990s, the effects of meshing conditions on dynamic behavior in torsional model was analyzed [13]. The influence of the ring support stiffness on free vibration was discussed, and potentially dangerous frequencies for sun gear-planet and planet-ring gear contacts were determined [14, 15]. In addition, the natural frequency and vibration mode sensitivities to system parameters were investigated for both tuned (cyclically symmetric) and mistuned planetary gears [16]. Other studies of

planetary gear dynamics include mesh stiffness variation and load sharing [17, 18], influence of free vibration [19, 20], and tooth crack detection [21–23]. These studies are not meant to provide multistage dynamic analysis; indeed, some research crosses into one- or two-stage analysis.

In general, most studies focus on planetary chain system or the components of helicopter's main reducer. Few of them involve the whole transmission system of helicopter and the researches on the impact of torsional stiffness of shaft on the dynamic response are rarely published yet. Therefore, in the paper, first of all, dynamics modeling is conducted on the four-stage helicopter transmission system; the differential equation of system vibration is deduced; the dynamic response corresponded by each DOF is calculated; then, the influence of the changes of torsional stiffness on amplitude of dynamic response is explored. Finally, the key shafts affecting each branch of the helicopter are analyzed by sensitivity analysis method, and theoretical support could be provided for the design of the helicopter.

2. Four-Stage Helicopter Main Reducer and Transmission

The model of four-stage deceleration helicopter's transmission system is shown in Figure 1 [24]. Figure 1 is reproduced from Yuan Chen et al. (2017) [under the Creative Commons Attribution License/public domain]. The model configuration is based upon EH101 helicopter, and the symbols and their meanings are shown in Nomenclature. The system has three same input branches, namely, j branch ($j = 1, 2, 3$). Each branch has 5 gears, which is $\theta_1, \theta_2, \ldots, \theta_5$. The rotational DOF of each gear pair is listed in Table 1. All shafts are numbered in Table 2 and their torsional stiffness are defined and calculated as follows:

$$\begin{aligned} \varphi &= \frac{Tl}{GI_p}, \\ I_p &= \frac{\pi D^4}{32}\left(1 - \frac{d^4}{D^4}\right), \\ k &= \frac{T}{\varphi}. \end{aligned} \tag{1}$$

3. Transmission Model

Based on the description, the four-stage deceleration helicopter transmission system, with 3 branches in the 1st and 2nd stage, has 27 generalized coordinates X (rotational DOF) shown in matrix:

$$X = \left\{\theta_1^{(j)}, \theta_2^{(j)}, \theta_3^{(j)}, \theta_4^{(j)}, \theta_5^{(j)}, \theta_6, \theta_7, \theta_8, \theta_9, \theta_s, \theta_{pi}, \theta_c\right\}^T. \tag{2}$$

The expansion formula of transmission error and time-varying meshing stiffness is shown in Fourier series under fundamental meshing frequency:

$$\begin{aligned} k(t) &= k_m + k_a \sin(\omega t + \varphi), \\ e(t) &= e_m + e_a \sin(\omega t + \varphi), \end{aligned}$$

$$\begin{aligned} e_{spi}(t) &= A_{spi} \sin\left(\omega t + \varphi_{spi}\right) + E_{pi} \sin\left(\omega_p t + \varphi_{pi} + \alpha\right) \\ &\quad + E_s \sin\left[\omega_s t + \varphi_s - \frac{2\pi(i-1)}{N} + \alpha\right], \\ e_{cpi}(t) &= A_{cpi} \sin\left(\omega t + \varphi_{cpi}\right) + E_{pi} \sin\left(\omega_p t + \varphi_{pi} - \alpha\right) \\ &\quad + E_c \sin\left[\omega_c t + \varphi_c - \frac{2\pi(i-1)}{N} - \alpha\right]. \end{aligned} \tag{3}$$

The relative displacement of each gear pair along the meshing line is defined as follows:

$$\begin{aligned} X_{a_b}(t) &= \theta_a r_a - \theta_b r_b - e_{ab}(t), \\ X_{spi}(t) &= \theta_s r_s - \theta_{pi} r_{pi} - e_{spi}(t), \\ X_{cpi}(t) &= \theta_{pi} r_{pi} - \theta_c r_c - e_{cpi}(t). \end{aligned} \tag{4}$$

Dynamic meshing and damping forces of each gear pair are defined as follows:

$$\begin{aligned} F_{a\_b}(t) &= k_{a\_b}(t) X_{a\_b} + c_{a\_b}(t) \dot{X}_{a\_b}, \\ F_{spi}(t) &= k_{spi}(t) X_{spi} + c_{spi}(t) \dot{X}_{spi}, \\ F_{cpi}(t) &= k_{cpi}(t) X_{cpi} + c_{cpi}(t) \dot{X}_{cpi}. \end{aligned} \tag{5}$$

According to the derivation, the differential equation of the four-stage main transmission system can be deduced through Newton's law, as shown below:

(1) Differential equation of motion for three input branches is

$$\begin{aligned} &J_1 \ddot{\theta}_1^{(j)} + \left[F_{1\_2}^{p(j)}(t) + F_{1\_2}^{d(j)}(t)\right] r_1 + k_{\text{in}} \theta_1^{(j)} = T_{\text{in}^{(j)}}, \\ &J_2 \ddot{\theta}_2^{(j)} - \left[F_{1\_2}^{p(j)}(t) + F_{1\_2}^{d(j)}(t)\right] r_2 + k_{23}^{(j)} \left(\theta_2^{(j)} - \theta_3^{(j)}\right) \\ &\quad = 0, \\ &J_3 \ddot{\theta}_3^{(j)} + \left[F_{3\_4}^{p(j)}(t) + F_{3\_4}^{d(j)}(t)\right] r_3 + k_{23}^{(j)} \left(\theta_3^{(j)} - \theta_2^{(j)}\right) \\ &\quad = 0, \\ &J_4 \ddot{\theta}_4^{(j)} - \left[F_{3\_4}^{p(j)}(t) + F_{3\_4}^{d(j)}(t)\right] r_4 + k_{45}^{(j)} \left(\theta_4^{(j)} - \theta_5^{(j)}\right) \\ &\quad = 0, \\ &J_5 \ddot{\theta}_5^{(j)} + \left[F_{5\_6}^{p(j)}(t) + F_{5\_6}^{d(j)}(t)\right] r_5 + k_{45}^{(j)} \left(\theta_5^{(j)} - \theta_4^{(j)}\right) \\ &\quad = 0. \end{aligned} \tag{6}$$

(2) Differential equation of motion for tail branch is

$$\begin{aligned} &J_6 \ddot{\theta}_6 - \sum_{j=1}^{3} \left[F_{5_6}^{p(j)}(t) + F_{5_6}^{d(j)}(t)\right] r_6 \\ &\quad + \left[F_{6_7}^{p}(t) + F_{6_7}^{d}(t)\right] r_6 + k_{6s}\left(\theta_6 - \theta_s\right) = 0, \\ &J_7 \ddot{\theta}_7 - \left[F_{6_7}^{p}(t) + F_{6_7}^{d}(t)\right] r_7 + k_{78}\left(\theta_7 - \theta_8\right) = 0, \end{aligned}$$

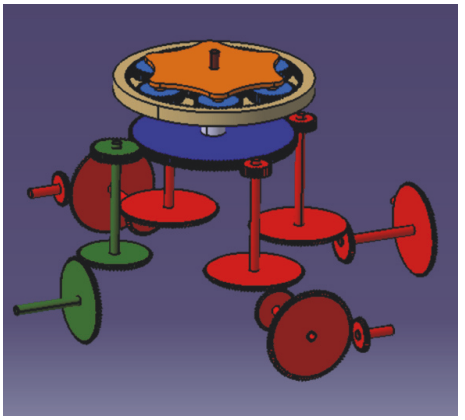

(a) 3D model

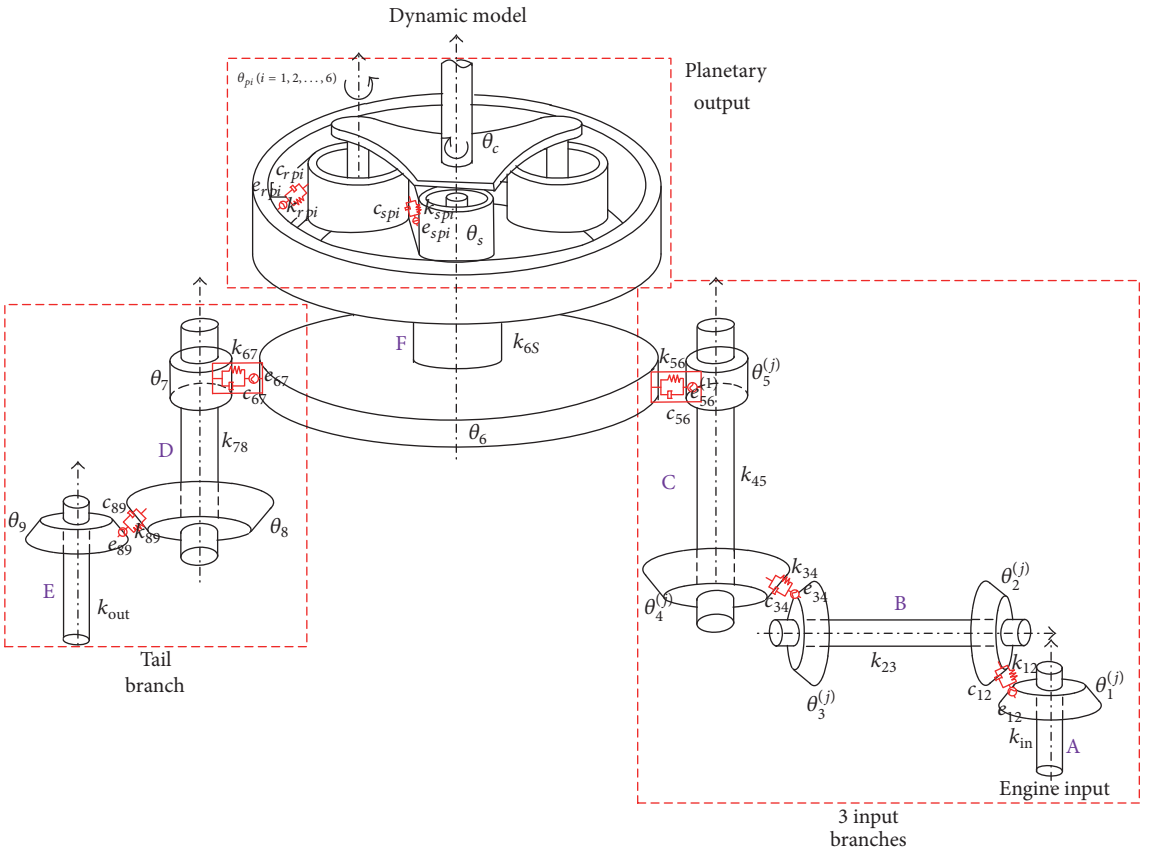

(b) Dynamic model

Figure 1: Model of three-engine helicopter's transmission system.

$$J_8\ddot{\theta}_8 + \left[F^p_{8\_9}(t) + F^d_{8\_9}(t)\right] r_8 + k_{78}(\theta_8 - \theta_7) = 0,$$
$$J_9\ddot{\theta}_9 - \left[F^p_{8_9}(t) + F^d_{8_9}(t)\right] r_9 + k_{\text{out}}\theta_9 = -T_r. \tag{7}$$

(3) Differential equation of motion for planetary output is

$$J_s\ddot{\theta}_s + \sum_{i=1}^{N}\left(F^p_{spi} + F^d_{spi}\right) r_s - k_{6s}(\theta_6 - \theta_s) = 0,$$
$$J_p\ddot{\theta}_{pi} - \left(F^p_{spi} + F^d_{spi}\right) r_p + \left(F^p_{cpi} + F^d_{cpi}\right) r_p = 0,$$
$$\left[J_c + \sum_{i=1}^{N}\left(m_{pi}r_c^2\right)\right]\ddot{\theta}_c - \sum_{i=1}^{N}\left(F^p_{spi} + F^d_{spi} + F^p_{cpi} + F^d_{cpi}\right) r_c \cos\alpha = -T_c. \tag{8}$$

In addition, after the decomposition and recombination, differential equation can be expressed with following matrix-vector form:

$$[M]\left\{\ddot{X}\right\} + [C]\left\{\dot{X}\right\} + [K]\{X\} = \{F\}. \tag{9}$$

Table 1: Name of torsional DOF.

DOF	Name
(1)	Gear 1 (first engine)
(2)	Gear 2 (first engine)
(3)	Gear 3 (first engine)
(4)	Gear 4 (first engine)
(5)	Gear 5 (first engine)
(6)	Gear 1 (second engine)
(7)	Gear 2 (second engine)
(8)	Gear 3 (second engine)
(9)	Gear 4 (second engine)
(10)	Gear 5 (second engine)
(11)	Gear 1 (third engine)
(12)	Gear 2 (third engine)
(13)	Gear 3 (third engine)
(14)	Gear 4 (third engine)
(15)	Gear 5 (third engine)
(16)	Gear 6 (synthesized gear)
(17)	Gear 7 (tail transmission)
(18)	Gear 8 (tail transmission)
(19)	Gear 9 (tail transmission)
(20)	Gear 10 (sun gear)
(21)	Gear 11 (planet gear 1)
(22)	Gear 12 (planet gear 2)
(23)	Gear 13 (planet gear 3)
(24)	Gear 14 (planet gear 4)
(25)	Gear 15 (planet gear 5)
(26)	Gear 16 (planet gear 6)
(27)	Planet carrier

External excitation and dynamic response are in kth-order Fourier series [25]:

$$F_k = \{A_1\}_k \sin \omega_k t + \{A_2\}_k \cos \omega_k t,$$
$$\{\Delta x\}_k = \{B_1\}_k \sin \omega_k t + \{B_2\}_k \cos \omega_k t. \quad (10)$$

Here $\{B_1\}_k$ and $\{B_1\}_k$ could be solved by the following equation:

$$\begin{bmatrix} -\omega_k^2 [M] + \left[\overline{K}\right] & -\omega_k [C] \\ \omega_k [C] & -\omega_k^2 [M] + \left[\overline{K}\right] \end{bmatrix} \begin{Bmatrix} \{B_1\}_k \\ \{B_2\}_k \end{Bmatrix} = \begin{Bmatrix} \{A_1\}_k \\ \{A_2\}_k \end{Bmatrix}. \quad (11)$$

The dynamic response of the system is linear superposition of the results corresponded by each order:

$$\{\Delta x(t)\} = \sum_{k=1}^{5} \left\{ \{B_1\}_k \sin \omega_k t + \{B_2\}_k \cos \omega_k t \right\}. \quad (12)$$

4. Calculation and Discussion

4.1. Model Parameters and Dynamic Response Calculation. A set of basic parameters are extracted from a geared system, listed in Table 3. Gear number is based on Table 1. In addition, the maximum output power of three engines is 1000 kW, 1500 kW, and 2000 kW, respectively. Maximum output speed of the engines is 20000 r/min.

The dimensionless amplitude is used to compare and understand how each gear response is affected by the system dynamics. Here, the dimensionless response amplitude is defined as the ratio of dynamic response to the amplitude of Gear 1, so all gears could be directly compared with system input gear.

By Fourier series method, the torsional displacement of each DOF can be obtained, as is shown in Figure 2. It indicates that the response of each gear pair is in the performance of periodic change under many dynamic factors like time-varying meshing stiffness and transmission error.

Figures 2(a) and 2(b) show response of first-stage gear pair; due to transmission error, they have slightly response difference. Figures 2(c) and 2(d) show response of second stage gear pair; Figures 2(e) and 2(f) show response of third stage gear pair. Figures 2(g), 2(h), and 2(i) show response of gear pairs in tail branch. Figures 2(j), 2(k), and 2(l) show response of gear pairs in planet train. The response amplitude increases constantly along with transmission path, in this case; Figure 2(l) shows the largest response amplitude.

4.2. Analysis of Dynamic Response Influenced by Torsional Stiffness of Shafts. The input three branches are the important branches of the four-stage transmission system. The structure is the same, but the internal excitation and external excitation are of difference, so their response amplitudes are distinctive.

Moreover, response amplitudes vary with torsional stiffness of shafts, as is shown in Figure 3. According to Figure 3(a), the response amplitude of three input branches decreases with the torsional stiffness of shaft A, but the change rate is very large when the torsional stiffness is less than 9×10^4 N·m/rad. But when the input shaft torsional stiffness is more than 4×10^5 N·m/rad, the change rate is small and tends to be stable. With respect to the other two shafts of the input branch (shaft B and shaft C), it can be seen from Figures 3(b)-3(c) that the response amplitudes of the three branches are also reduced with increasing torsional stiffness; however, the decline rate is relatively stable with no obvious turning point. Based on Figures 3(d) and 3(e), the torsional stiffness of two shafts in tail branch has no effect on the three-branch input response. From Figure 3(f), it can be seen that the response amplitude of three input branches decreases linearly with input shaft of sun gear, and the amplitude of 3rd input branch is the largest and 2nd one is the smallest.

It can be seen from Figure 3 that response of the 3rd input branch is larger than the other two branches due to the different magnitude of the external excitation. Therefore, when designing the 3rd input shaft, the shaft with larger torsional stiffness should be selected.

Four-stage deceleration helicopter's transmission system has multiple branches of input and output, and the dynamic

Table 2: Name of shafts.

Shaft number	Shaft name	Torsional Stiffness	Calculated value (N·m/rad)
A	Input shaft	k_{in}	30×10^4
B	Gear 2 and Gear 3 connecting shaft	k_{23}	60×10^4
C	Gear 4 and Gear 5 connecting shaft	k_{45}	30×10^4
D	Gear 7 and Gear 8 connecting shaft	k_{78}	60×10^4
E	Tail shaft	k_{out}	20×10^4
F	Sun gear input shaft	k_{6s}	90×10^4

Table 3: Gear parameters of four-stage main transmission system.

	Tooth number	Module	Face width (mm)	Transmission error (μm)	Initial phase of transmission error (°)	Initial phase of meshing stiffness (°)
Gear 1	30	4.5	40	50	0	0
Gear 2	85	4.5	40	50	0	0
Gear 3	40	5	60	30	20	20
Gear 4	90	5	60	30	20	20
Gear 5	25	4.75	40	40	30	30
Gear 6	142	4.75	40	40	30	30
Gear 7	40	5	35	20	0	0
Gear 8	60	5	35	20	0	0
Gear 9	70	5	40	40	20	20
Gear 10	68	5	40	40	20	20
Gear 11–16	37	5	40	30	$\varphi_{sp1} = 0$, $\varphi_{sp2} = 240$, $\varphi_{sp3} = 180$, $\varphi_{sp4} = 150$, $\varphi_{sp5} = 180$, $\varphi_{sp6} = 240$	$\varphi_{sp1} = 0$, $\varphi_{sp2} = 60$, $\varphi_{sp3} = 120$, $\varphi_{sp4} = 150$, $\varphi_{sp5} = 180$, $\varphi_{sp6} = 240$

response in key branches of the transmission chain is normally different. Response amplitudes of key branches vary with torsional stiffness of shafts, as is depicted in Figure 4.

The carrier shows the maximum amplitude and varies intensively with torsional stiffness of shaft F. The response amplitudes of three input branches decrease obviously due to the rising stiffness of shaft C. The tail branch decreases obviously with the torsional stiffness of shaft D. In conclusion, the response amplitude of each branch decreases with increasing torsional stiffness. The reduced amplitudes are related to their sensitivity coefficients, so sensitivity calculation and analysis are required to be carried out.

4.3. Key Branches Influenced by Torsional Stiffness of Shafts. Sensitivity analysis is generally used to study the key variables in the system of many uncertainties. In this paper, based on the mutative torsional stiffness of the shaft, sensitivity analysis is used to find the key shafts which affect the response characteristics of each branch. The sensitivity coefficient of the shafts is analyzed in calculation to provide engineering reference for the design of helicopter's shafts in four-stage main transmission system.

The sensitivity of each branch's response $x(t)$ corresponding to torsional stiffness k is defined as follows [26]:

$$S_k^x = \left| \frac{\left(x' - x\right)/x}{\left(k' - k\right)/k} \right| \times 100\%, \tag{13}$$

where x and x' are corresponding response amplitude before and after the change of stiffness k; k and k' are the torsional stiffness values before and after the change, respectively.

In Figure 5(a), for the input three branches, their sensitivity to the shaft C is about 49% (2nd input branch has maximum sensitivity); their sensitivity to the shaft B is approximately 30% (3rd input branch has maximum sensitivity); their sensitivity to the shaft A is nearly 11% (2nd input branch has maximum sensitivity). So shaft C is the key shaft of the input branches. It could also been seen in Figure 5(b) that tail branch has the highest value in sensitivity with shaft D (45%) and with shaft E secondly (38%); however this branch has little sensitivity with shafts of input branch (shafts A, B, and C), along with shaft F in the planet system. Figure 5(c) depicts that planetary system has 75% sensitive value with shaft F, which makes it a key shaft to this branch. In

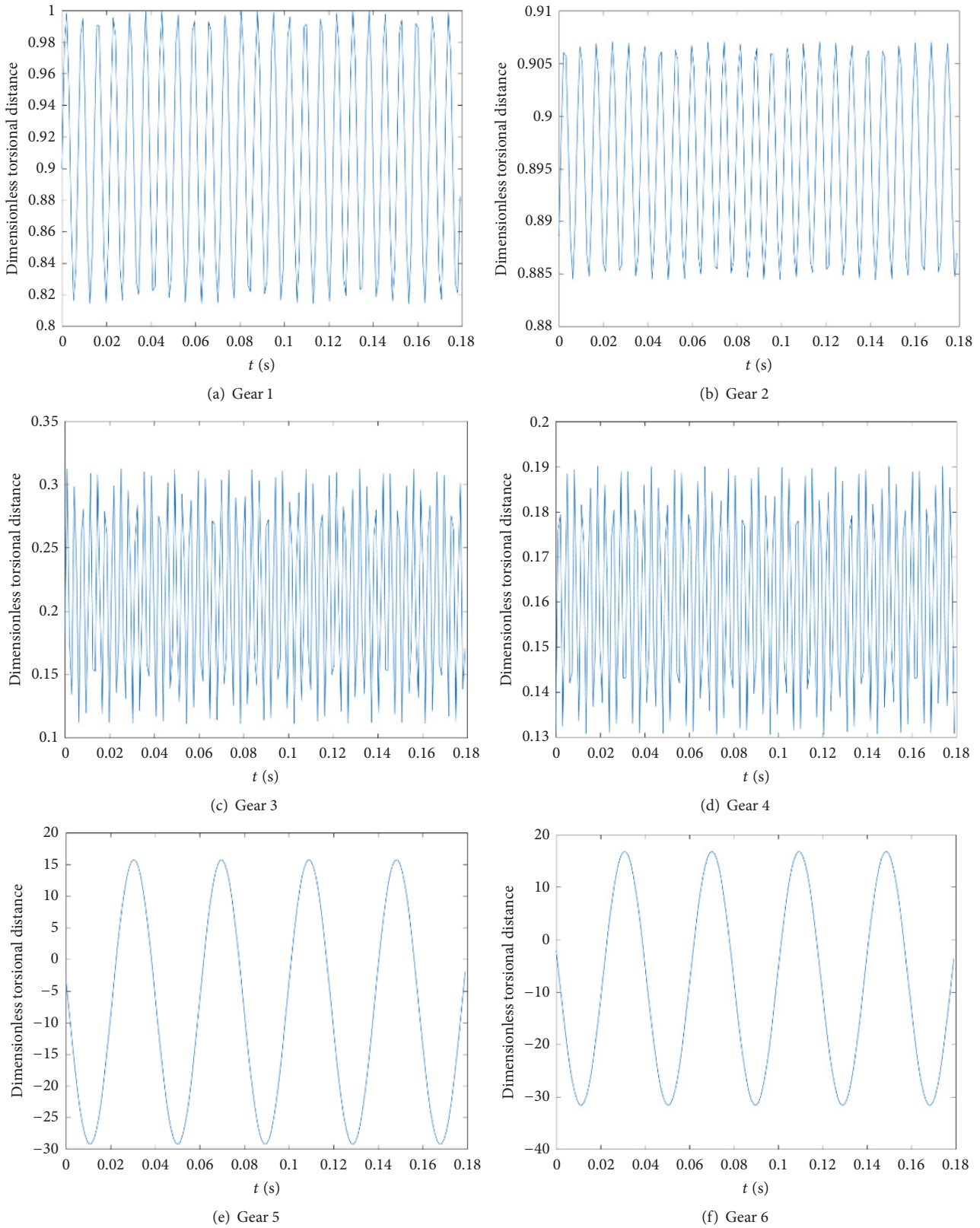

Figure 2: Continued.

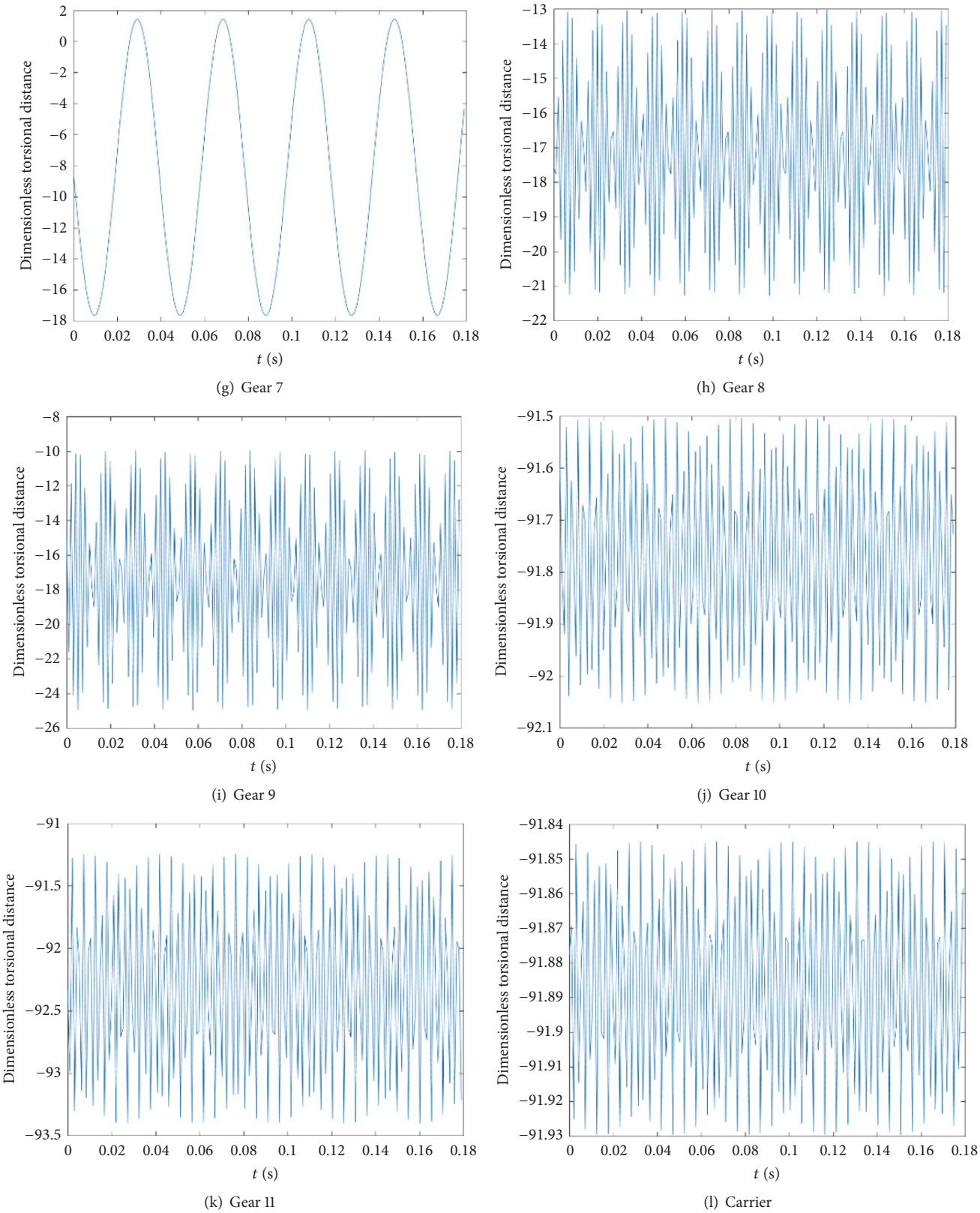

Figure 2: Dynamic response of gears in helicopter transmission system.

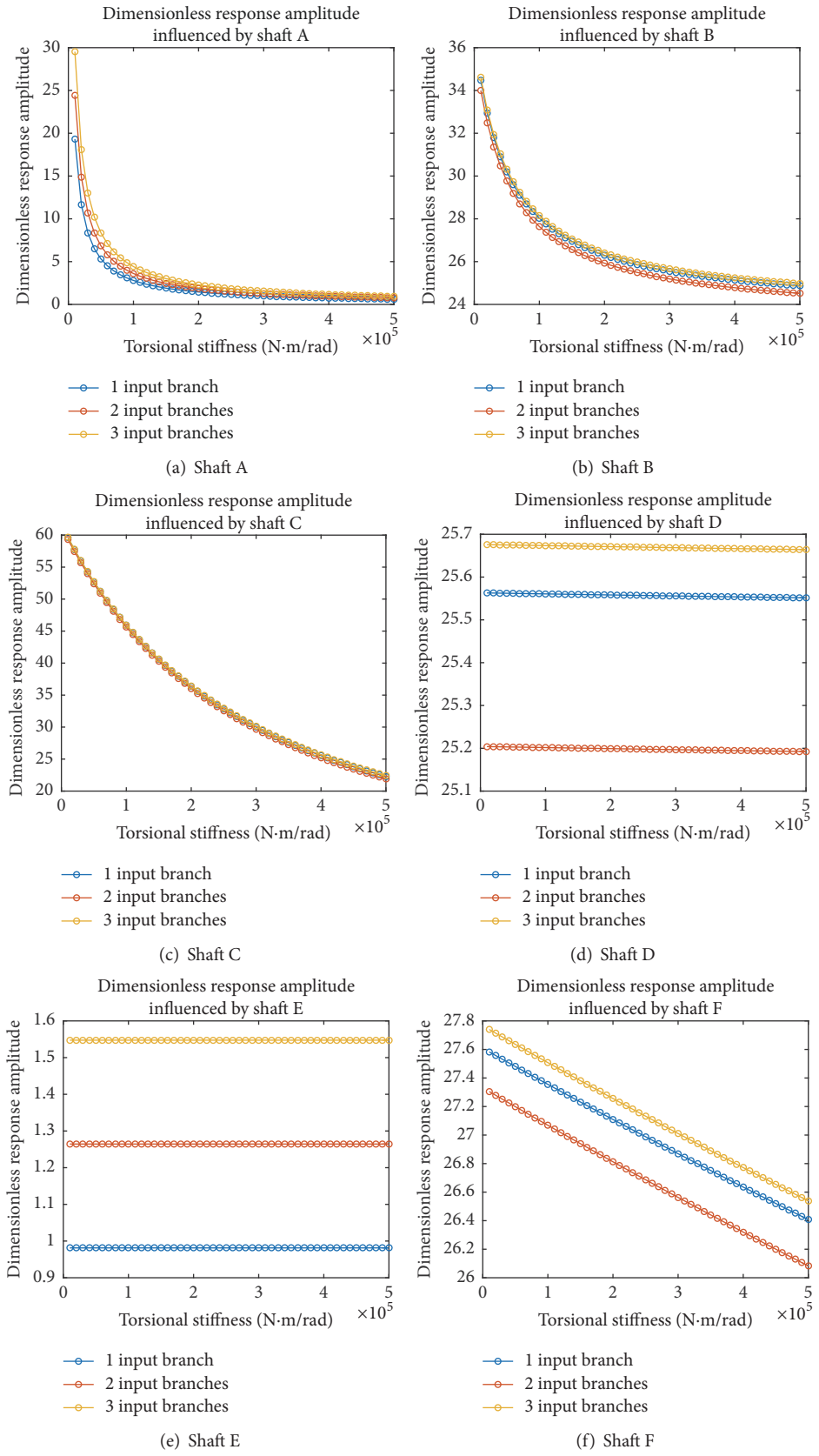

Figure 3: Response amplitude influenced by torsional stiffness of input shafts.

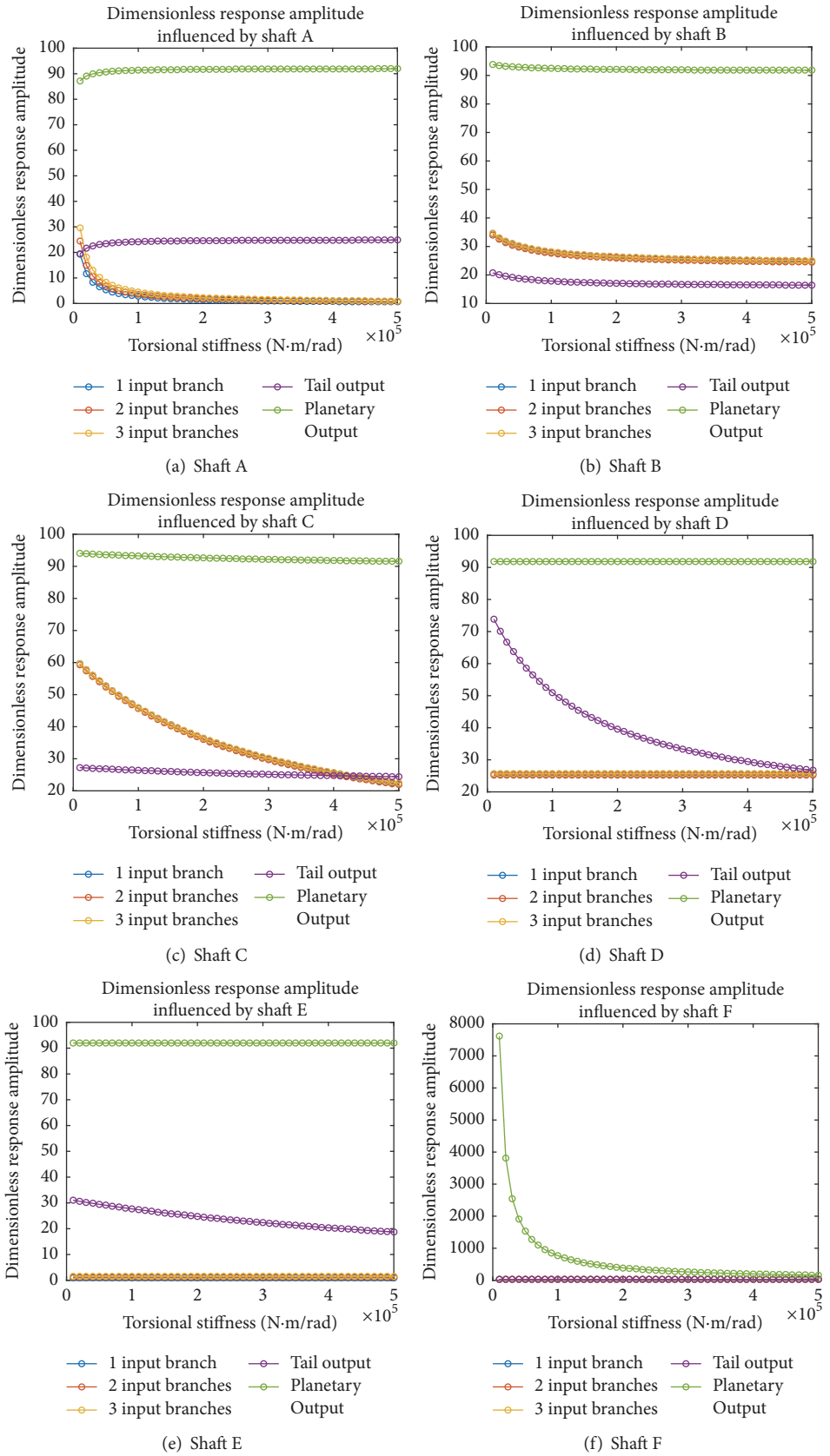

Figure 4: Response amplitude influenced by torsional stiffness of shafts in the system.

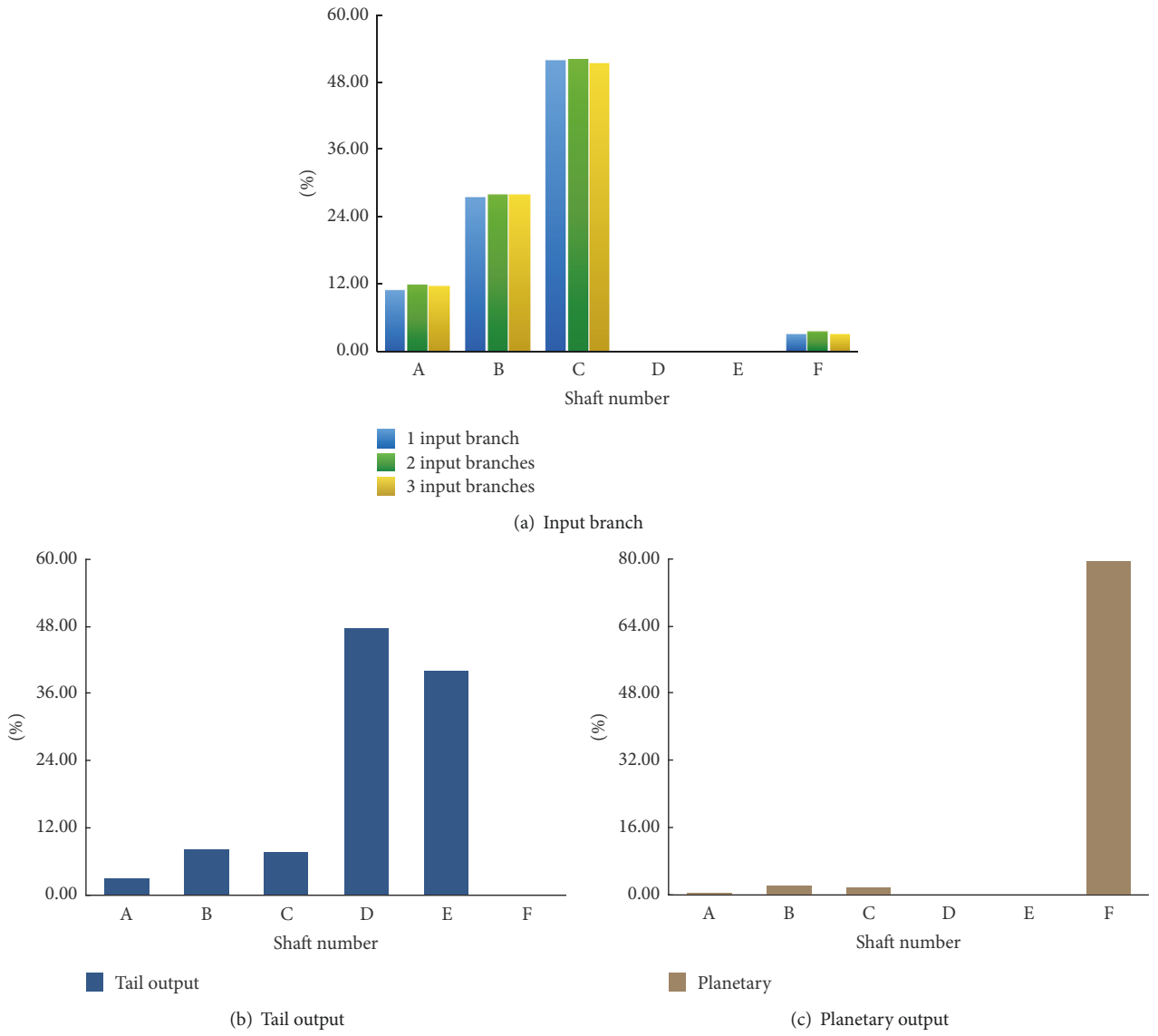

Figure 5: Sensitivity of shafts in the system.

general, the shaft within each branch is more sensitive to the branch itself and less sensitive to other branches according to the Figure 5.

5. Conclusion

In this paper, a new dynamics model of four-stage helicopter transmission system is proposed and the differential governing equation of system vibration is derived as well. Based on the governing equation, time-domain dynamic characteristics are obtained by employing the Fourier series method. Moreover, this paper presents the influence of the changes of torsional stiffness on dynamic response.

The analysis results based on the ideal modal enable us to draw the following conclusions:

(1) The output response of carrier and tail branch is relatively larger, which is related to the increasing torque in the last stage. In other words, the last stage should be designed carefully.

(2) The response amplitudes of the three input branches decrease with the increase of torsional stiffness of the input shaft in the system. The 3rd input response is larger than the other two input branches, so when designing its input shaft, a shaft with larger torsional stiffness should be taken into consideration.

(3) The amplitude of response of each branch is on the decrease when torsional stiffness rises, and the decrease magnitude is associated with its sensitivity coefficient. When the stiffness increases to a certain value, the response amplitude tends to be a stable value.

(4) The key shaft of the three input branches is C shafts; the tail branch response is the most sensitive to the

D shaft, and the E shaft is the second; the planetary chain system shows more sensitivity to the F shaft.

Nomenclature

$c(t)$: Mesh damping
$[C]$: Damping matrix
d: Internal diameter of the shaft
D: External diameter of the shaft
e: Transmission error
e_a: Dynamic transmission error
e_m: Static transmission error
$[F]$: External excitation matrix
$F(t)$: Dynamic forces of each gear pair
G: Shear elastic modulus
j: Number of input engines ($j = 1, 2, 3$)
$[K]$: Stiffness matrix
k: Meshing stiffness
k_m: Average variable meshing stiffness
k_a: Maximum variable meshing stiffness
$[M]$: Mass matrix
N: Number of planets
r: Radius of base circle
T: Torque
$X(t)$: Relative displacement along the meshing line
$\overline{X}$: Dimensionless displacement along the meshing line
$\dot{X}$: Relative velocity along the meshing line
α: Pressure angle
β: Initial phase of meshing stiffness
θ: Rotational DOF
φ: Initial phase of transmission error
ω: Fundamental meshing frequency.

Subscripts

c: Carrier
in: Input branch
r: Tail branch
pi: Planet gear i ($i = 1, 2, \ldots, 6$)
s: Sun gear.

Conflicts of Interest

The authors declare that there are no conflicts of interest regarding the publication of this paper.

Acknowledgments

The work described in this paper is fully supported by the National Natural Science Foundation of PRC (Grants nos. 51775265 and 51475226); Postgraduate Research and Practice Innovation Program of Jiangsu Province; China Scholarship Council's Support for Joint Research with Professor Yeping Xiong in University of Southampton; China Association for Science & Technology and Nanjing University of Aeronautics and Astronautics Ph.D. Visiting Program. The authors acknowledges the project of "Dynamic Analysis on Four-Stage Main Transmission System" (Grant no. KYCX17_0242) for supplying the gear data.

References

[1] D. B. Stringer, P. N. Sheth, and P. E. Allaire, "A new helicopter transmission model for condition-based maintenance technologies using first principles," in *Proceedings of the 45th AIAA/ASME/SAE/ASEE Joint Propulsion Conference and Exhibit*, August 2009.

[2] P. Dempsey, J. Keller, and D. Wade, "Signal detection theory applied to helicopter transmission diagnostic thresholds," 2008.

[3] P. J. Dempsey, D. G. Lewicki, and D. D. Le, "Investigation of current methods to identify helicopter gear health," in *Proceedings of the 2007 IEEE Aerospace Conference*, USA, March 2007.

[4] D. G. Astridge, "Helicopter transmissions—design for safety and reliability," *Proceedings of the Institution of Mechanical Engineers, Part G: Journal of Aerospace Engineering*, vol. 203, no. 2, pp. 123–138, 1989.

[5] M. Kubur, A. Kahraman, D. M. Zini, and K. Kienzle, "Dynamic analysis of a multi-shaft helical gear transmission by finite elements: model and experiment," *Journal of Vibration and Acoustics*, vol. 126, no. 3, pp. 398–406, 2004.

[6] J. Huang, S. Zhang, and Y. Zhang, "The Influences of System Parameters on the Natural Characteristics of a Parallel Multi-Shaft," in *Gear-Rotor System , Machinery Design Manufacture, no.7*, pp. 15–17, in Chinese, 7, 2013.

[7] I. Valiente-Blanco, C. Cristache, J. Sanchez-Garcia-Casarrubios, F. Rodriguez-Celis, and J.-L. Perez-Diaz, "Mechanical Impedance Matching Using a Magnetic Linear Gear," *Shock and Vibration*, vol. 2017, Article ID 7679390, 2017.

[8] F.-J. Lv, "Vibration analysis of gear drive system based on whole transfer matrix method," *Applied Mechanics and Materials*, vol. 340, pp. 69–74, 2013.

[9] X. Jin, X. Guan, L. Zhao, H. Wang, and Z. Sun, "An analysis on performance of high-speed gear dynamics based on transfer-matrix method," *Advanced Materials Research*, vol. 415-417, pp. 621–624, 2012.

[10] J. Lin and R. G. Parker, "Sensitivity of planetary gear natural frequencies and vibration modes to model parameters," *Journal of Sound and Vibration*, vol. 228, no. 1, pp. 109–128, 1999.

[11] C.-S. Chen, S. Natsiavas, and H. D. Nelson, "Coupled lateral-torsional vibration of a gear-pair system supported by a squeeze film damper," *Journal of Vibration and Acoustics*, vol. 120, no. 4, pp. 860–867, 1998.

[12] G. D. Jennings, R. G. Harley, and D. C. Levy, "Sensitivity of Subsynchronous Resonance Predictions to Turbo-Generator Modal Parameter Values and to Omitting Certain Active Subsynchronous Modes," *IEEE Power Engineering Review*, vol. 7, no. 9, p. 50, 1987.

[13] A. Kahraman, "Planetary gear train dynamics," *Journal of Mechanical Design*, vol. 116, no. 3, pp. 713–720, 1994.

[14] A. Saada and P. Velex, "Extended model for the analysis of the dynamic behavior of planetary trains," *Transactions of the ASME—Journal of Mechanical Design*, vol. 117, no. 2, pp. 241–247, 1995.

[15] T. M. Ericson and R. G. Parker, "Experimental measurement of the effects of torque on the dynamic behavior and system parameters of planetary gears," *Mechanism and Machine Theory*, vol. 74, pp. 370–389, 2014.

[16] J. Lin and R. G. Parker, "Analytical characterization of the unique properties of planetary gear free vibration," *Journal of Vibration and Acoustics*, vol. 121, no. 3, pp. 316–321, 1999.

[17] V. Batinic, "Determination of gear mesh stiffness in planetary gearing," *Vojnotehnicki glasnik*, vol. 56, no. 2, pp. 227–236, 2008.

[18] D.-P. Sheng, R.-P. Zhu, G.-H. Jin, F.-X. Lu, and H.-Y. Bao, "Dynamic load sharing characteristics and sun gear radial orbits of double-row planetary gear train," *Journal of Central South University*, vol. 22, no. 10, pp. 3806–3816, 2015.

[19] L. Zhang, Y. Wang, K. Wu, R. Sheng, and Q. Huang, "Dynamic modeling and vibration characteristics of a two-stage closed-form planetary gear train," *Mechanism and Machine Theory*, vol. 97, pp. 12–28, 2016.

[20] S. Zhou, G. Song, M. Sun, and Z. Ren, "Nonlinear dynamic response analysis on gear-rotor-bearing transmission system," *Journal of Vibration and Control*.

[21] X. H. Liang, M. J. Zuo, and M. R. Hoseini, "Vibration signal modeling of a planetary gear set for tooth crack detection," *Engineering Failure Analysis*, vol. 48, pp. 185–200, 2015.

[22] X. Liang, M. J. Zuo, and L. Liu, "A windowing and mapping strategy for gear tooth fault detection of a planetary gearbox," *Mechanical Systems and Signal Processing*, vol. 80, pp. 445–459, 2016.

[23] Z. Li, X. Yan, X. Wang, and Z. Peng, "Detection of gear cracks in a complex gearbox of wind turbines using supervised bounded component analysis of vibration signals collected from multi-channel sensors," *Journal of Sound and Vibration*, vol. 371, pp. 406–433, 2016.

[24] A. Bianchi and S. Rossi, "Modeling and finite element analysis of a complex helicopter transmission including housing, shafts and gears," 1997.

[25] M. Li and L. Yu, "Analysis of the coupled lateral torsional vibration of a rotor-bearing system with a misaligned gear coupling," *Journal of Sound and Vibration*, vol. 243, no. 2, pp. 283–300, 2001.

[26] J. V. Milanović, C. P. N. Fu, R. Radosavljević, and Z. Lazarević, "Sensitivity of torsional modes and torques to uncertainty in shaft mechanical parameters," *Electric Power Components and Systems*, vol. 29, no. 10, pp. 867–881, 2001.